Int J Adv Manuf Technol (2014) 72:1361–1376
DOI 10.1007/s00170-014-5685-y

ORIGINAL ARTICLE

An experimental study on motion error of hexarot parallel manipulator

Mohammad Reza Chalak Qazani · Siamak Pedrammehr · Arash Rahmani · Mehran Shahryari · Aslan Khani Sheykh Rajab · Mir Mohammad Ettefagh

Received: 22 October 2013 / Accepted: 31 January 2014 / Published online: 15 March 2014

Abstract In this paper, a novel 6-DOF parallel manipulator with coaxial actuated arms is introduced and investigated. This mechanism has six rotating arms, and by rotation of arms about the base, positioning and desired movement of the mechanism is achieved. Sine parallel mechanisms have a nonlinear motion while moving from an initial position to a desired position, investigation of nonlinear error in such mechanisms is of paramount importance. In this paper, inverse and forward kinematics of the mechanism are studied. Nonlinear error of the mechanism's motion in its workspace is extracted using mid-oscillating circle and kinematic relations as well. Moreover, effective parameters on nonlinear motion error of mechanism are determined. The results obtained by theoretical method are further verified through image processing experimental tests. It is found that the results of the theoretical analysis and experimental test are in good consistency.

Keywords Parallel mechanism · Hexarot · Kinematics · Nonlinear error · Image processing

M. R. Chalak Qazani (✉)
Faculty of Technology & Engineering, Department of Mechanical Engineering, Tarbiat Modares University, Tehran, Iran
e-mail: m.r.chalakqazani@gmail.com

S. Pedrammehr
Faculty of Engineering and Natural Sciences, Sabanci University, Tuzla, Istanbul, Turkey

M. Shahryari
Faculty of Engineering, Ahar Branch, Islamic Azad University, Ahar, Iran

A. Khani Sheykh Rajab
Department of Mechanical Engineering, Ilkhchi Branch, Islamic Azad University, Ilkhchi, Iran

A. Rahmani · M. M. Ettefagh
Faculty of Mechanical Engineering, University of Tabriz, Tabriz, Iran

1 Introduction

The general demand on the mechanism design lies primarily in the high acceleration capability of the mechanism axes while at the same time meeting the high demands on accuracy [1]. Currently, most of the mechanisms are designed on the basis of using simple open kinematic chain. Such multiaxes mechanisms suffer from the disadvantage that each axis must either move or carry all other axes that are situated further along the kinematic chain. In order to overcome this weakness, parallel mechanism has found extensive application in the industry. The accuracy is among the primary requirements for all mechanisms. This needs a thorough understanding of the tool path programming. The purpose of the present study was to partially meet this need and fill the gap existing in the literature in this respect.

Both the inverse and forward kinematics of parallel mechanisms exhibit nonlinear behaviors. In the inverse kinematics, the pods' lengths do not change linearly with a linear path travelled by the platform [2–4]. In the forward kinematics, when pods are actuated linearly, the platform moves along a nonlinear path. This makes the path control and interpolation functions in parallel mechanisms become more complex than in serial manipulators. Zheng et al. [5] investigated path control for a novel 5-DOF parallel mechanism. They demonstrated the nonlinearity of both inverse and forward kinematics of the mechanism, they proposed a novel interpolation algorithm, and however they did not elaborate the nonlinearity of the mechanism. Beale [6] made the first serious attempt to measure nonlinearity and proposed four measures of nonlinearity. This problem has been tackled in several research works. Guttman and Meeter [7] showed that Beale's measures tend to predict that a model will behave linearly even when considerable nonlinearity is present. Box [8] presented a formula for estimating the bias in the LS estimators. Using simulation studies, Gillis and Ratkowsky [9] found that this formula not only predicted bias to the correct order of magnitude in yield density models but also gave a good indication of the

extent of nonlinear behavior of the model as well. Bates and Watts [10] developed new measures of nonlinearity based on the geometric concept of curvature. They utilized the maximum relative intrinsic and parameter effects curvatures of the solution locus for estimating the extent of nonlinearity. They showed that the projections of the straight and equispaced parametric lines in the parameter space onto the plane tangent to the solution locus are, in general, neither straight nor equispaced. Karimi and Nategh [11] employed Bates and Watts' measures of nonlinearity to investigate the nonlinearity of the forward kinematics. They demonstrated that the length of the region, defined as the linear approximation of the lifted line, has a significant impact on the nonlinearity of the mechanism. Dasgupta and Mruthyunjaya [12] developed an algorithm for singularity-free path planning of the Stewart platform manipulator. The limitations of their algorithm were its lack of confidence in detecting the nonexistence of a singularity-free path and its sensitivity to intersections of singularity hypersurfaces. Shaw and Chen [13] investigated an algorithm for generating the cutting path of a parallel kinematic machine. Iso-scallop method and genetic algorithm are utilized respectively in the process of generating the cutting path and finding the configurations of the tool without a singular position in their research work. Merlet [14] investigated trajectory verification for a classical Gough-Stewart platform. In his study, the real-time method has been developed and errors have been controlled. Pugazhenthi et al. [15] developed an optimal trajectory planning algorithm for a parallel kinematic machine during contour machining. They developed a code to maximize the stiffness of the structure and minimize the force requirement of the actuator, and the constraints of workplace and singularity have been taken into account in their study. Dash et al. [16] presented a numerical technique for path planning within the workspace of parallel manipulators. Isolated singularities have been eliminated through local routing method based on Grassmann's line geometry in their study. Afroun et al. [17, 18] presented a technique for generating optimal motion for a parallel DELTA robot and Gough parallel robot. In their study, the sequential programming quadratic method has been applied to find the optimal position of the spline control points. Harib et al. [19] developed an analytical model for trajectory planning of a redundant hybrid machine tool structure consisting of a Stewart platform and a two-degree-of-freedom rotary tilting table. Having presented eight coordinates, they defined five coordinates through conventional part programming and other three coordinates via trajectory planning. Li [20] investigated reconfiguration and tool path planning of hexapod machine tools. In his study, appropriate trajectory planning is considered to reduce a nonlinear error in the path. Jinsong et al. [21] utilized kinematic nonlinearity of parallel machine tools to investigate their interpolation accuracy.

In this paper, inverse and forward kinematic relations of hexarot mechanism are developed. By having instantaneous velocity and acceleration in any point, it is possible to obtain error. Therefore, nonlinear error of the mechanism's motion in its workspace is extracted using mid-oscillating circle and kinematic relations as well. Effective parameters on nonlinear motion error of mechanism are also determined. The results obtained by theoretical method are also examined through image processing. It is found that the results of theoretical analysis and experimental test are in good consistency.

2 Description of hexarot mechanism

The mechanism under investigation consists of a triangular platform, a cylindrical base column, and six actuated rotating arms with coinciding axes of rotation (Fig. 1). Each arm connects by a 5-DOF link to a manipulated platform at its connection point U_i (i=1 to 6). The platform is triangular, and the three pairs of joints on the rotating arms approximately form a triangle. The two triangles compose the two sides of an octahedron. There are six actuated rotational joints R_i between the central cylindrical base column and the upper arms a_i. Each upper arm is connected to a lower arm l_i by a spherical joint S_i. There are six universal joints U_i between the lower arm l_i and the manipulated platform. The location and orientation of the moving platform frame $\{\mathbf{P}\}$ is specified according to the base frame $\{\mathbf{W}\}$. $\mathbf{a}_i$ and $\mathbf{l}_i$ are respectively the length vectors of the upper and lower arms in the base frame of the reference. The physical specifications of the manipulator are presented in the Appendix.

The actuators are placed on the base column, and since the lower arms are not susceptible to bending or torsion, their design can be lightweight. Hence, the total moving mass of the octahedral hexarot is low. The proposed mechanism has six manipulated DOFs. Since the upper arms can rotate indefinitely around the base column, its positional workspace is comparatively large for a parallel manipulator. The arrangement of the joints on the manipulated platform and the upper arms reduces the risk of collisions between the lower arm links and enables a sizable range of platform rotations. With careful choice of structural parameters, this manipulator can also achieve favorable isotropic properties [22, 23]. The possibility of using identical drivelines, identical upper arms, and identical lower arm links ensures that the number of different components can be kept low, which would reduce the cost of manufacturing of the manipulator. Hexarot could be useful in haptics or for work inside cylindrical spaces, such as repair work inside pipes, positioning, or assembly tasks inside the body of an airplane.

3 Inverse kinematics

Inverse kinematic problem of the platform involves determination of the rotation, angular velocity, and

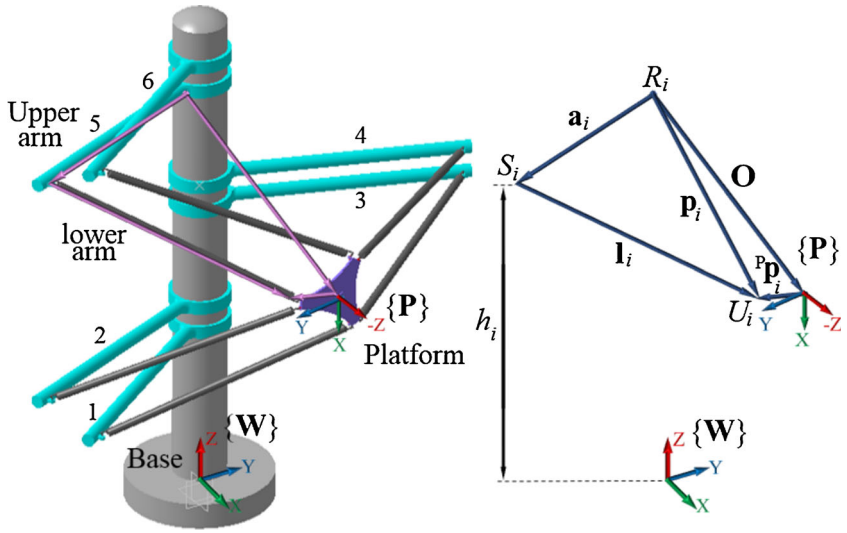

Fig. 1 The hexarot manipulator

acceleration of six arms through considering a specified position, velocity, and acceleration of the moving platform center.

Considering a vectorial representation of the mechanism, position vector of the *i*th spherical joint with the reference in base frame, $\mathbf{a}_i$, can be obtained as follows:

$$\mathbf{a}_i = [\, a_i \cos\varphi_i \quad a_i \sin\varphi_i \quad h_i \,]^{\mathrm{T}} \tag{1}$$

where φ_i is the angle between the *i*th upper arm and *X*-axis of the reference frame $\{\mathbf{W}\}$ and indicates the rotation of the *i*th upper arm around the base column.

Considering the moving platform as an equilateral triangle, and taking into account s_1 as the length of its sides and s_2 as the distance between the universal joint and the vertex, the position of each universal joint, ${}^{\mathrm{P}}\mathbf{p}_i$, with reference in frame $\{\mathbf{P}\}$ can be presented as follows:

$${}^{\mathrm{P}}\mathbf{p}_i = \begin{bmatrix} (s_1-s_2)/2 & s_2/2 & (s_1-2s_2)/2 & -(s_1-2s_2)/2 & -s_2/2 & -(s_1-s_2)/2 \\ (-s_1+3s_2)/2\sqrt{3} & (2s_1-3s_2)/2\sqrt{3} & -s_1/2\sqrt{3} & -s_1/2\sqrt{3} & (2s_1-3s_2)/2\sqrt{3} & (-s_1+3s_2)/2\sqrt{3} \\ 0 & 0 & 0 & 0 & 0 & 0 \end{bmatrix} \tag{2}$$

These vectors can be expressed in the base frame of reference by a translation and rotation transformation as follows:

$$\mathbf{p}_i = \mathbf{O} + \mathbf{R}\ {}^{\mathrm{P}}\mathbf{p}_i \tag{3}$$

in which $\mathbf{O}$ is the position vector of the geometrical center of the moving platform in base frame and $\mathbf{R}=\mathbf{R}_{ZYZ}$ is the rotation matrix which can be obtained as:

$$\mathbf{R} = \begin{bmatrix} \cos\theta_1\ \cos\theta_2\ \cos\theta_3 - \sin\theta_1\ \sin\theta_3 & -\cos\theta_1\ \cos\theta_2\ \sin\theta_3 - \sin\theta_1\ \cos\theta_3 & \cos\theta_1 \sin\theta_2 \\ \sin\theta_1\ \cos\theta_2\ \cos\theta_3 + \cos\theta_1\ \sin\theta_3 & -\sin\theta_1\ \cos\theta_2\ \sin\theta_3 + \cos\theta_1 \cos\theta_3 & \sin\theta_1 \sin\theta_2 \\ -\sin\theta_2\ \cos\theta_3 & \sin\theta_2\ \sin\theta_3 & \cos\theta_2 \end{bmatrix} \tag{4}$$

in which θ_1, θ_2, and θ_3 are the Euler angles.

The length of the *i*th lower arm, l_i, can be expressed as follows:

$$l_i^2 = |\mathbf{p}_i - \mathbf{a}_i|^2 \tag{5}$$

Substituting Eqs. (1) and (3) into Eq. (5) gives the following equation:

$$d_{i1} + d_{i2} \sin\varphi_i + d_{i3} \cos\varphi_i = 0 \tag{6}$$

in which

$$\begin{aligned} d_{i1} = {} & x^2 + y^2 + (z-h_i)^2 - l_i^2 + a_i^2 + p_{ix}^2 + p_{iy}^2 + p_{iz}^2 + 2(z-h_i)\, p_{iz} \cos\theta_2 \\ & -2(z-hi)\ \ p_{ix} \sin\theta_2 \cos\theta_3 + 2z(z-hi)\ \ p_{iy} \sin\theta_2 \sin\theta_3 \\ & -2x\ \ \left(p_{ix} \sin\theta_1 \sin\theta_3 + p_{iy} \sin\theta_1 \cos\theta_3 - piz \cos\theta_1 \sin\theta_2\right) \\ & + 2y\left(p_{ix} \cos\theta_1 \sin\theta_3 + p_{iy} \cos\theta_1 \cos\theta_3 + p_{iz} \sin\theta_1 \sin\theta_2\right) \\ & + 2x \cos\theta_1 \cos\theta_2 \cos\theta_3 (p_{ix} - piy) + 2yp_{ix} \sin\theta_1 \cos\theta_2 \cos\theta_3 \\ & -2yp_{iy} \sin\theta_1 \cos\theta_2 \sin\theta_3 \end{aligned} \tag{7}$$

$$\begin{aligned} d_{i2} = {} & -2a_i\Big(y + p_{ix} \cos\theta_1 \sin\theta_3 + p_{iy} \cos\theta_1 \cos\theta_3 + p_{iz} \sin\theta_1 \sin\theta_2 \\ & + p_{ix} \sin\theta_1 \cos\theta_2 \cos\theta_3 - p_{iy} \sin\theta_1 \cos\theta_2 \sin\theta_3\Big) \end{aligned} \tag{8}$$

$$\begin{aligned} d_{i3} = {} & -2a_i\Big(x - p_{ix} \sin\theta_1 \sin\theta_3 - p_{iy} \sin\theta_1 \cos\theta_3 + p_{iz} \cos\theta_1 \sin\theta_2 \\ & + p_{ix} \cos\theta_1 \cos\theta_2 \cos\theta_3 - p_{iy} \cos\theta_1 \cos\theta_2 \sin\theta_3\Big) \end{aligned} \tag{9}$$

φ_i can be obtained by substituting Eqs. (7), (8), and (9) into Eq. (6), which yields the following equation:

$$\begin{aligned} \varphi_i &= -2\arctan\left[\left(d_{i2} - \sqrt{-d_{i1}^2 + d_{i2}^2 + d_{i3}^2}\right)/d_{i1} - d_{i3}\right] \text{for } i = 1,2,5,6 \\ \varphi_i &= -2\arctan\left[\left(d_{i2} + \sqrt{-d_{i1}^2 + d_{i2}^2 + d_{i3}^2}\right)/d_{i1} - d_{i3}\right] \text{for } i = 3,4 \end{aligned} \tag{10}$$

Considering Eq. (3), $\mathbf{a}_i$ can be obtained as follows:

$$\mathbf{l}_i = \mathbf{O} + \mathbf{R}^{\mathrm{P}}\mathbf{p}_i - \mathbf{a}_i \tag{11}$$

Considering $\mathbf{n}_i$ as the unit vector of the ith lower arm (i.e., $\mathbf{l}_i = l_i\mathbf{n}_i$) and maximizing Eq. (11) to the power of 2 and then taking the derivative with respect to time on both sides of the resulting equation, yields the following equation:

$$(\mathbf{n}_i \times \mathbf{a}_i)\ .\ \dot{\varphi}_i = \dot{\mathbf{X}} \cdot \mathbf{n}_i + (\mathbf{n}_i \times \mathbf{p}_i) \cdot \boldsymbol{\omega} \tag{12}$$

where $\dot{\mathbf{X}}$ and $\boldsymbol{\omega}$ are respectively the linear and angular velocity of the moving platform center in the base frame. $\dot{\varphi}_i$ is also the angular velocity of the ith upper arm.

The angular velocity is only in the Z-direction. Therefore, only the Z parameter of $(\mathbf{n}_i \times \mathbf{a}_i)$ will be considered in the dot product of $\dot{\varphi}_i$. By considering na_{zi} as the Z parameter of $(\mathbf{n}_i \times \mathbf{a}_i)$, this parameter can be defined as follows:

$$na_{zi} = a_i n_{iy} \cos\varphi_i - a_i n_{ix} \sin\varphi_i \tag{13}$$

The angular velocity of the ith upper arm can be obtained by substituting Eq. (13) into Eq. (12), which yields the following equation:

$$\dot{\boldsymbol{\varphi}} = \mathbf{J}^{-1}\begin{bmatrix} \dot{\mathbf{X}} \\ \boldsymbol{\omega} \end{bmatrix} \tag{14}$$

in which $\mathbf{J}^{-1}$ is the inverse Jacobian matrix and can be expressed as follows:

$$\mathbf{J}^{-1} = \begin{bmatrix} (\mathbf{n}_1/na_{z1})^{\mathrm{T}} & (\mathbf{n}_1 \times \mathbf{p}_1/na_{z1})^{\mathrm{T}} \\ \vdots & \vdots \\ (\mathbf{n}_6/na_{z6})^{\mathrm{T}} & (\mathbf{n}_6 \times \mathbf{p}_6/na_{z6})^{\mathrm{T}} \end{bmatrix}_{6\times 6} \tag{15}$$

Taking the product of the two sides of Eq. (14) with na_{zi} and then taking the derivative with respect to time on both sides of the resulting equation, the angular acceleration of the ith upper arm, $\ddot{\varphi}_i$, can be calculated from the following equation:

$$\begin{aligned} & \ddot{\varphi}_i\left(a_i n_{iy} \cos\varphi_i - a_i n_{ix} \sin\varphi_i\right) - \dot{\varphi}_i\Big(a_i n_{ix}\dot{\varphi}_i \cos\varphi_i + a_i n_{iy}\dot{\varphi}_i \sin\varphi_i\Big) \\ & + \dot{\varphi}_i\left(a_i n_{ix}\omega_{lzi} \cos\varphi_i + a_i n_{iy}\omega_{lzi} \sin\varphi_i - a_i n_{iz}\omega_{lyi} \sin\varphi_i - a_i n_{iz}\omega_{lxi} \cos\varphi_i\right) \\ & = \mathbf{J}^{-1}\begin{bmatrix} \ddot{\mathbf{X}} \\ \boldsymbol{\alpha} \end{bmatrix} + \frac{\mathrm{d}\mathbf{J}^{-1}}{\mathrm{d}t}\begin{bmatrix} \dot{\mathbf{X}} \\ \boldsymbol{\omega} \end{bmatrix} \end{aligned} \tag{16}$$

where $\ddot{\mathbf{X}}$ and $\boldsymbol{\alpha}$ are respectively the linear and angular acceleration of the moving platform center in the base frame of reference and $\boldsymbol{\omega}_{li} = \begin{bmatrix} \omega_{lxi} & \omega_{lyi} & \omega_{lzi} \end{bmatrix}^{\mathrm{T}}$ is the angular velocity of the ith lower arm.

4 Forward kinematics

The forward kinematic problem of the platform is determination of the position, velocity, and acceleration of the moving platform center through considering a specified rotation, angular velocity, and acceleration of the six arms. Therefore, in forward kinematics, unknown parameters are divided in to two groups of position and orientation of the moving platform. Therefore, there will be six unknown parameters which are x, y, z, θ_1, θ_2, and θ_3.

By substituting Eqs. (7), (8), and (9) into Eq. (6), the function $f_i(x_n)$ can be expressed as follows:

$$\begin{aligned} f_i(x_n) = \varepsilon_i = {} & x^2 + y^2 + (z-h_i)^2 - l_i^2 + a_i^2 + p_{ix}^2 + p_{iy}^2 + p_{iz}^2 + 2(z-h_i)\,p_{iz}\cos\theta_2 \\ & -2(z-h_i)\;p_{ix}\sin\theta_2\cos\theta_3 + 2z(z-h_i)\;p_{iy}\sin\theta_2\sin\theta_3 \\ & -2x\;\left(p_{ix}\sin\theta_1\sin\theta_3 + p_{iy}\sin\theta_1\cos\theta_3 - p_{iz}\cos\theta_1\sin\theta_2\right) \\ & +2y\;\left(p_{ix}\cos\theta_1\sin\theta_3 + p_{iy}\cos\theta_1\cos\theta_3 + p_{iz}\sin\theta_1\sin\theta_2\right) \\ & +2x\cos\theta_1\cos\theta_2\cos\theta_3\left(p_{ix} - p_{iy}\right) + 2yp_{ix}\sin\theta_1\cos\theta_2\cos\theta_3 \\ & -2yp_{iy}\sin\theta_1\cos\theta_2\sin\theta_3 - 2a_i\sin\varphi_i\left(y + p_{ix}\cos\theta_1\sin\theta_3 + p_{iy}\cos\theta_1\cos\theta_3\right. \\ & \left. + p_{iz}\sin\theta_1\sin\theta_2 + p_{ix}\sin\theta_1\cos\theta_2\cos\theta_3 - p_{iy}\sin\theta_1\cos\theta_2\sin\theta_3\right) \\ & -2a_i\cos\varphi_i\left(x - p_{ix}\sin\theta_1\sin\theta_3 - p_{iy}\sin\theta_1\cos\theta_3 + p_{iz}\cos\theta_1\sin\theta_2\right. \\ & \left. + p_{ix}\cos\theta_1\cos\theta_2\cos\theta_3 - p_{iy}\cos\theta_1\cos\theta_2\sin\theta_3\right) \end{aligned} \tag{17}$$

in which ε_i is the error for coordination of the ith joint. The output of forward kinematics is $\mathbf{X} = [x \;\; y \;\; z \;\; \theta_1 \;\; \theta_2 \;\; \theta_3]^{\mathrm{T}}$. By replacing the value of $\mathbf{X}$ in Eq. (17), the evaluation function is determined, and the more $\mathbf{X}$ approaches to its real value, the more the function approaches to zero, so that error stays in the desired domain. Regarding six rotating joints, it should be noted that Eq. (17) must be used for calculation of each joint.

In this study, for solving the equation, the Newton-Raphson method [24, 25] is utilized, because this method only needs repeating the prior calculation. This feature leads to stability of the calculations and also leads to convergence of the method to final answer in less time and with less error.

$$f_i(x) = f_i'(x)[x_{n+1} - x_n] \tag{18}$$

where x_n are the available values and x_{n+1} are the values obtained from the available values. $f_i'(x)$ is the fractional derivative of evaluating function which can be calculated as follows:

$$f_i'(x_n) = \frac{\partial f_i(x_n)}{\partial x_n} = \frac{\partial \varepsilon_i}{\partial x_n} = \begin{bmatrix} \frac{\partial \varepsilon_1}{\partial x_n} & \frac{\partial \varepsilon_1}{\partial y_n} & \frac{\partial \varepsilon_1}{\partial z_n} & \frac{\partial \varepsilon_1}{\partial \theta_{1n}} & \frac{\partial \varepsilon_1}{\partial \theta_{2n}} & \frac{\partial \varepsilon_1}{\partial \theta_{3n}} \\ \vdots & \vdots & \vdots & \vdots & \vdots & \vdots \\ \frac{\partial \varepsilon_6}{\partial x_n} & \frac{\partial \varepsilon_6}{\partial y_n} & \frac{\partial \varepsilon_6}{\partial z_n} & \frac{\partial \varepsilon_6}{\partial \theta_{1n}} & \frac{\partial \varepsilon_6}{\partial \theta_{2n}} & \frac{\partial \varepsilon_6}{\partial \theta_{3n}} \end{bmatrix}_{6\times 6} \tag{19}$$

which yields the following equations:

$$\begin{aligned} \frac{\partial \varepsilon_i}{\partial x} = {} & 2x - 2p_{ix}\sin\theta_1\sin\theta_3 - 2p_{iy}\sin\theta_1\cos\theta_3 + 2p_{iz}\cos\theta_1\sin\theta_2 \\ & + 2p_{ix}\cos\theta_1\cos\theta_2\cos\theta_3 - 2p_{iy}\cos\theta_1\cos\theta_2\sin\theta_3 - 2a_i\cos\varphi_i \end{aligned} \tag{20}$$

$$\begin{aligned} \frac{\partial \varepsilon_i}{\partial y} = {} & 2y - 2p_{ix}\cos\theta_1\sin\theta_3 - 2p_{iy}\cos\theta_1\cos\theta_3 + 2p_{iz}\sin\theta_1\sin\theta_2 \\ & + 2p_{ix}\sin\theta_1\cos\theta_2\cos\theta_3 - 2p_{iy}\sin\theta_1\cos\theta_2\sin\theta_3 - 2a_i\sin\varphi_i \end{aligned} \tag{21}$$

$$\begin{aligned} \frac{\partial \varepsilon_i}{\partial z} = {} & 2z - 2h_i + 2p_{iz}\cos\theta_2 + 2p_{iy}\sin\theta_2\sin\theta_3 - 2p_{iz}\cos\theta_1\sin\theta_2 \\ & - 2p_{ix}\cos\theta_1\cos\theta_2\cos\theta_3 \end{aligned} \tag{22}$$

$$\begin{aligned} \frac{\partial \varepsilon_i}{\partial \theta_1} = {} & 2x\;\left(p_{ix}\cos\theta_1\sin\theta_3 - p_{iy}\cos\theta_1\cos\theta_3 - p_{iz}\sin\theta_1\sin\theta_3\right) \\ & -2y\left(p_{ix}\sin\theta_1\sin\theta_3 + p_{iy}\sin\theta_1\cos\theta_3 - p_{iz}\cos\theta_1\sin\theta_2\right) \\ & + 2y\cos\theta_1\cos\theta_2\cos\theta_3\left(p_{ix} - p_{iy}\right) - 2xp_{ix}\sin\theta_1\cos\theta_2\cos\theta_3 \\ & + 2xp_{iy}\sin\theta_1\cos\theta_2\sin\theta_3 + 2a_i\sin\varphi_i\left(p_{ix}\sin\theta_1\sin\theta_3 + p_{iy}\sin\theta_1\cos\theta_3\right. \\ & \left. - p_{iz}\cos\theta_1\sin\theta_2 - p_{ix}\cos\theta_1\cos\theta_2\cos\theta_3 + p_{iy}\cos\theta_1\cos\theta_2\sin\theta_3\right) \\ & + 2a_i\cos\varphi_i\left(p_{ix}\cos\theta_1\sin\theta_3 + p_{iy}\cos\theta_1\cos\theta_3 + p_{iz}\sin\theta_1\sin\theta_2\right. \\ & \left. + p_{ix}\sin\theta_1\cos\theta_2\cos\theta_3 - p_{iy}\sin\theta_1\cos\theta_2\cos\theta_3\right) \end{aligned} \tag{23}$$

$$\begin{aligned} \frac{\partial \varepsilon_i}{\partial \theta_2} = {} & 2p_{iz}(h_i - z)\;\sin\theta_2 + 2xp_{iz}\cos\theta_1\cos\theta_2 + 2yp_{iz}\sin\theta_1\cos\theta_2 \\ & + 2zp_{ix}\cos\theta_2\cos\theta_3 + 2zp_{iy}\cos\theta_1\sin\theta_3 + 2h_ip_{ix}\cos\theta_2\cos\theta_3 \\ & -2h_ip_{iy}\cos\theta_2\sin\theta_3 - 2xp_{ix}\cos\theta_1\sin\theta_2\cos\theta_3 \\ & + 2xp_{iy}\cos\theta_1\sin\theta_2\sin\theta_3 - 2yp_{ix}\sin\theta_1\sin\theta_2\cos\theta_3 \\ & + 2yp_{iy}\sin\theta_1\sin\theta_2\sin\theta_3 \\ & -2a_i\sin\varphi_i(-p_{ix}\sin\theta_1\sin\theta_2\cos\theta_3 + p_{iy}\sin\theta_1\sin\theta_2\sin\theta_3 \\ & \qquad + p_{iz}\sin\theta_1\cos\theta_2) \\ & -2a_i\cos\varphi_i(-p_{ix}\cos\theta_1\sin\theta_2\cos\theta_3 + p_{iy}\cos\theta_1\sin\theta_2\sin\theta_3 \\ & \qquad + p_{iz}\cos\theta_1\cos\theta_2) \end{aligned} \tag{24}$$

$$\begin{aligned} \frac{\partial \varepsilon_i}{\partial \theta_3} = {} & -2xp_{ix}\cos\theta_1\cos\theta_3 + 2xp_{iy}\sin\theta_1\sin\theta_3 + 2yp_{ix}\cos\theta_1\cos\theta_3 \\ & -2yp_{iy}\cos\theta_1\sin\theta_3 - 2zp_{ix}\sin\theta_2\sin\theta_3 + 2zp_{iy}\sin\theta_2\sin\theta_3 \\ & -2h_ip_{ix}\sin\theta_2\sin\theta_3 - 2h_ip_{iy}\sin\theta_2\cos\theta_3 - 2xp_{ix}\cos\theta_1\cos\theta_2\sin\theta_3 \\ & -2xp_{iy}\cos\theta_1\cos\theta_2\cos\theta_3 - 2yp_{ix}\sin\theta_1\cos\theta_2\sin\theta_3 \\ & -2yp_{iy}\sin\theta_1\cos\theta_2\cos\theta_3 \\ & -2a_i\sin\varphi_i(p_{ix}\cos\theta_1\cos\theta_3 - p_{ix}\sin\theta_1\cos\theta_2\sin\theta_3 \\ & \qquad - p_{iy}\cos\theta_1\sin\theta_3 - p_{iy}\sin\theta_1\cos\theta_2\sin\theta_3) \\ & -2a_i\cos\varphi_i(p_{ix}\sin\theta_1\cos\theta_3 - p_{ix}\cos\theta_1\cos\theta_2\sin\theta_3 \\ & \qquad + p_{iy}\sin\theta_1\sin\theta_3 - p_{iy}\cos\theta_1\cos\theta_2\cos\theta_3) \end{aligned} \tag{25}$$

By substituting Eqs. (20) to (25) into Eq. (19) and then by substituting the resulting equation and Eq. (17) into Eq. (18), x_{n+1} can be calculated from x_n.

In this step, there are six linear equations and six unknown parameters in which using the Gauss-Jordan method, it is possible to obtain x_{n+1} from x_n. This repeating continues till the error get in the desired domain which is assumed to be 10^{-3} (millimeters) in this study.

Taking the product of the two sides of Eq. (14) with $na_{zi}\,\mathbf{J}$, gives the following equation:

$$\begin{bmatrix} \dot{\mathbf{X}} \\ \boldsymbol{\omega} \end{bmatrix} = na_{zi}\mathbf{J}\,\dot{\boldsymbol{\varphi}} \tag{26}$$

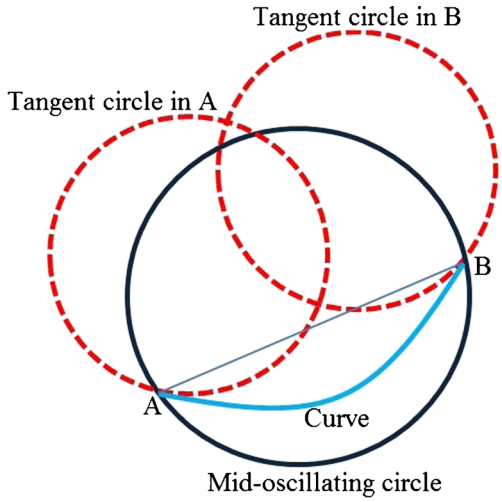

Fig. 2 Real and suitable paths

Therefore, using the Jacobian matrix, which is obtained from the position of the platform, and using the angular velocity of the spherical joints as well, it is possible to calculate the velocity of the moving platform center.

Considering

$$u_i = a_i n_{iy}\omega_{lzi}\sin\varphi_i - a_i n_{iz}\omega_{lyi}\sin\varphi_i + a_i n_{ix}\omega_{lzi}\cos\varphi_i - a_i n_{iz}\omega_{lxi}\cos\varphi_i - a_i n_{ix}\dot{\varphi}_i\cos\varphi_i - a_i n_{iy}\dot{\varphi}_i\sin\varphi_i \quad (27)$$

and taking the product of the two sides of Eq. (16) with **J**, gives the following equation:

$$\begin{bmatrix}\ddot{\mathbf{X}}\\ \boldsymbol{\alpha}\end{bmatrix} = \mathbf{J}\left(na_{zi}\ddot{\varphi}_i\right) + \mathbf{J}\left(u_i\dot{\varphi}_i\right) - \mathbf{J}\frac{\mathrm{d}\mathbf{J}^{-1}}{\mathrm{d}t}\begin{bmatrix}\dot{\mathbf{X}}\\ \boldsymbol{\omega}\end{bmatrix} \quad (28)$$

Therefore, using the Jacobian matrix, which is obtained from the moving platform position, and using the angular velocity and acceleration of the spherical joints as well as the velocity of the platform, it is possible to calculate the acceleration of the moving platform center.

5 Nonlinear error

In order to control the error in an acceptable range, the value of nonlinear error must be obtained. Here in this research, a mid-oscillating circle is utilized to obtain the kinematic error.

Oscillating circle of a curve abuts the curve at a point. In other words, it has the same tangent and curvature as the curve has at that point. Just as the tangent line is the best line for approximating a curve at a given point, the oscillating circle is the best circle that approximates the curve at a point. The radius of the osculating circle is simply the inverse of curvature. This, however, is of critical importance both in nonlinear motion of the platform and its path programming.

Curvatures vary throughout the whole path, and the radii of the oscillating circles at the start and end points of the path are different. Therefore, the radius of the mid-oscillating circle is taken into account in this research (Fig. 2).

The normal vector of the plane consisting of the mid-oscillating circle, **H**, can be presented as follows:

$$\mathbf{H} = \mathbf{L}\times\mathbf{N} = \begin{bmatrix} i & j & k\\ L_x & L_y & L_z\\ N_x & N_y & N_z\end{bmatrix} \quad (29)$$

where **L** is the vector connecting two interpolated points A and B and **N** is the unit vector which is normal to the tangent vector. **N** can be obtained as follows:

$$\mathbf{N} = \ddot{\mathbf{X}}/\left|\ddot{\mathbf{X}}\times\dot{\mathbf{X}}\right| \quad (30)$$

in which $\ddot{\mathbf{X}}$ and $\dot{\mathbf{X}}$ are respectively the linear velocity and acceleration vectors of the moving platform between A and B.

Since points A and B are in the plane with the normal vector **H**, the center of the circular path can be obtained by solving the system of nonlinear equations as follows:

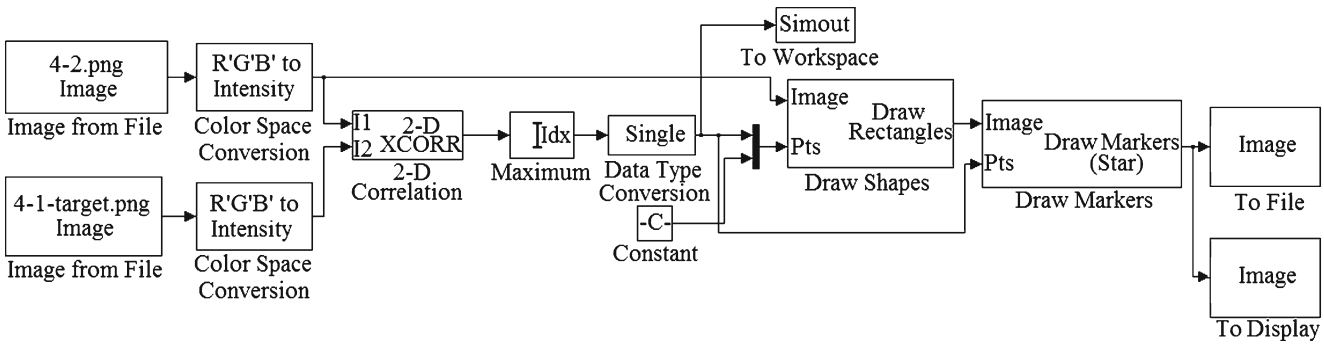

Fig. 3 Block diagram of image processing

Fig. 4 Image processing setup

$$\begin{cases} \left(L_x^{'}-C_x\right)^2+\left(L_y^{'}-C_y\right)^2+\left(L_z^{'}-C_z\right)^2=\rho^2 \\ \left(L_x^{''}-C_x\right)^2+\left(L_y^{''}-C_y\right)^2+\left(L_z^{''}-C_z\right)^2=\rho^2 \\ H_x(C_x-L_x)+H_y\left(C_y-L_y\right)+H_z(C_z-L_z)=0 \end{cases} \quad (31)$$

where $\mathbf{L}'=(L_x^{'},L_y^{'},L_z^{'})$ and $\mathbf{L}''=(L_x^{''},L_y^{''},L_z^{''})$ are respectively the position vectors of points A and B and $\mathbf{C}=(C_x, C_y, C_z)$ is the center of the mid-oscillating circle. ρ is the radius of the mid-oscillating circle and can be obtained as follows:

$$\rho=(\rho_A+\rho_B)/2 \quad (32)$$

ρ_A and ρ_B are respectively the radius of the oscillating circle at points A and B and can be defined as follows:

$$\rho_A=1/\kappa_A \quad (33)$$

$$\rho_B=1/\kappa_B \quad (34)$$

where κ_A and κ_B are the curvatures in points A and B, respectively. The curvature in these two points can be determined by kinematics of arms and platform.

Considering direct kinematic equations and substituting Eq. (31) into Eqs. (33) and (34), kinematic error equation can be written as follows:

$$e=\rho-\sqrt{\rho^2-(S/2)^2} \quad (35)$$

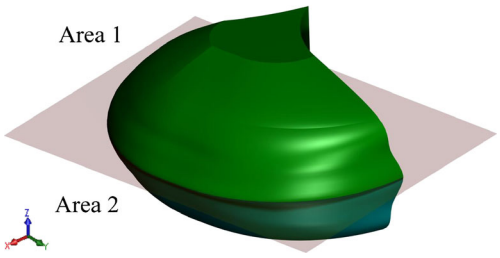

Fig. 5 Cross section of the workspace for hexarot in X=300 mm

where S is the length of the curve between two interpolated points A and B. If kinematic error exceeds acceptable range, S has to be mitigated. In this condition, changing S is of key importance in controlling the path length and kinematic error.

6 Experimental test

Image processing is one of the available methods for measuring the movement of various dynamic systems. In this method, using a camera, determined positions of target motion on the platform are captured. Photographs are imported to the MATLAB Image Processing Toolbox. First, this toolbox provides a matrix for each photo. The elements of this matrix are the amount of pixels in each photo. For each matrix element, numbers between 0 and 256 are selected by the software. For example, white and complete black have numbers 0 and 256, respectively. Target coordinate is imported to the software by the first photo. So the application finds the status of this small matrix in a larger matrix and it follows the motion in the next photos. Thus, in the end of the movement, motion coordinate is obtained in pixels. Finally, regarding the relationship between the number of pixels and targets diameters, using a coefficient, the equation of motion is obtained (Fig. 3).

For the test, two cameras are used in two directions in order to capture the target motion (Fig. 4). After photographing starts, the motion of the rotational joints between the upper arms and base are provided so that the moving platform and

Table 1 Different parameters considered as full factorial classes and levels

Classes	Workspace	S (mm)	X (mm)
Level 1	From areas 1 to 1	20	100
Level 2	From areas 1 to 2	40	200
Level 3	From areas 2 to 2	60	300
Level 4		80	400
Level 5		100	500

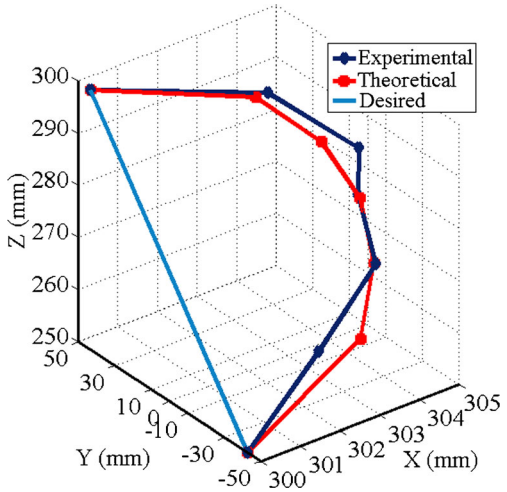

Fig. 6 The motion diagram of the platform center regardless of its nonlinear motion, S=200 mm, moving from areas 1 to 2, and X=300 mm

target on it starts to move. Camera numbers 1 and 2 record movements in the *YZ*- and *XZ*-planes, respectively. In order to make the camera lens perpendicular to the spherical target, the camera base is completely aligned with the ground level. To adjust the lens in the direction of the coordinate axes in the *XY*-plane, the platform target is moved in the *Y*- and *Z*-directions and the distance between the camera and target is measured. This distance is kept fixed in a perpendicular direction with rotating the camera and moving the platform. It should be noted that this process is performed for both cameras.

In this paper, two general conditions have been experimentally tested and results have been compared with each other. In the first case, the orientation of the platform is conserved. In the latter case, the rotation of the platform is taken into account.

Since the nonlinear error rate differs in various areas of the workspace, the workspace of the mechanism is of utmost importance in determining and controlling this error. Assuming a cross section of the workspace in the *X*-direction, and regarding the origin of coordinates which is at the center of the platform, one symmetrical plane with two areas can be considered within the workspace of the platform (Fig. 5).

Considering one symmetrical plane shown in Fig. 5, all motions within the workspace and with the specified distance from the base column can be provided with three motions.

One of the effective parameters is the *X*-direction of the workspace. The closer the distance to the base, the larger the curvature of the curve will be. In this paper, the parameter X is examined in five cases of 100, 200, 300, 400, and 500 mm.

The movement distance is the other parameter which affects the error rate. In a way that by increasing the movement distance, the error will increase. In this paper, the movement distance is examined in five cases of 20, 40, 60, 80, and 100 mm.

The test has three effective factors including the workspace, the distance to the base, and the movement distance. Workspace factor has three levels; however, the other factors have five levels (Table 1). Thus, full factorial of test equals to 75.

After considering the corresponding outputs of each camera, the motion diagram of the platform center will be obtained (Fig. 6). Having this motion diagram at hand, the nonlinear error can be calculated using the mid-oscillating circle. In Fig. 6, the distance from the platform center to the line obtained from the projection of its motion diagram on plane X=300 provides a nonlinear error in experimental testing.

7 Results and discussions

Neglecting the rotational motion of the platform, Fig. 7 illustrates the platform's motion error both theoretically and experimentally. The maximum difference between the results obtained from the experimental test and theoretical method is 1.1 mm. This, however, shows the accuracy of the results.

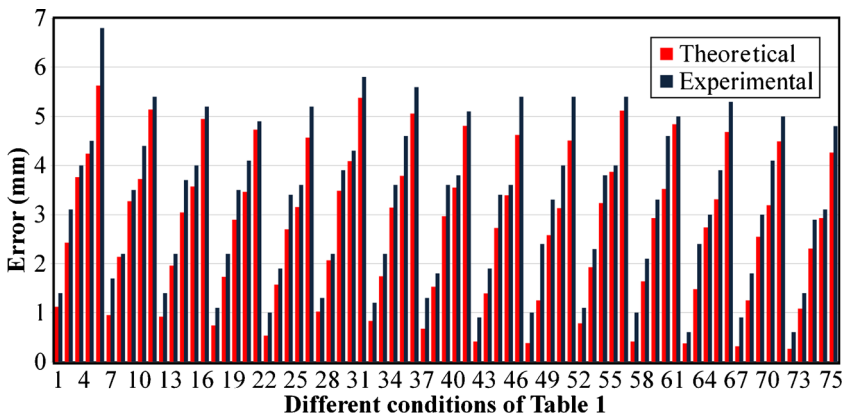

Fig. 7 Comparison of experimental and theoretical results by neglecting the nonlinear motion of the platform

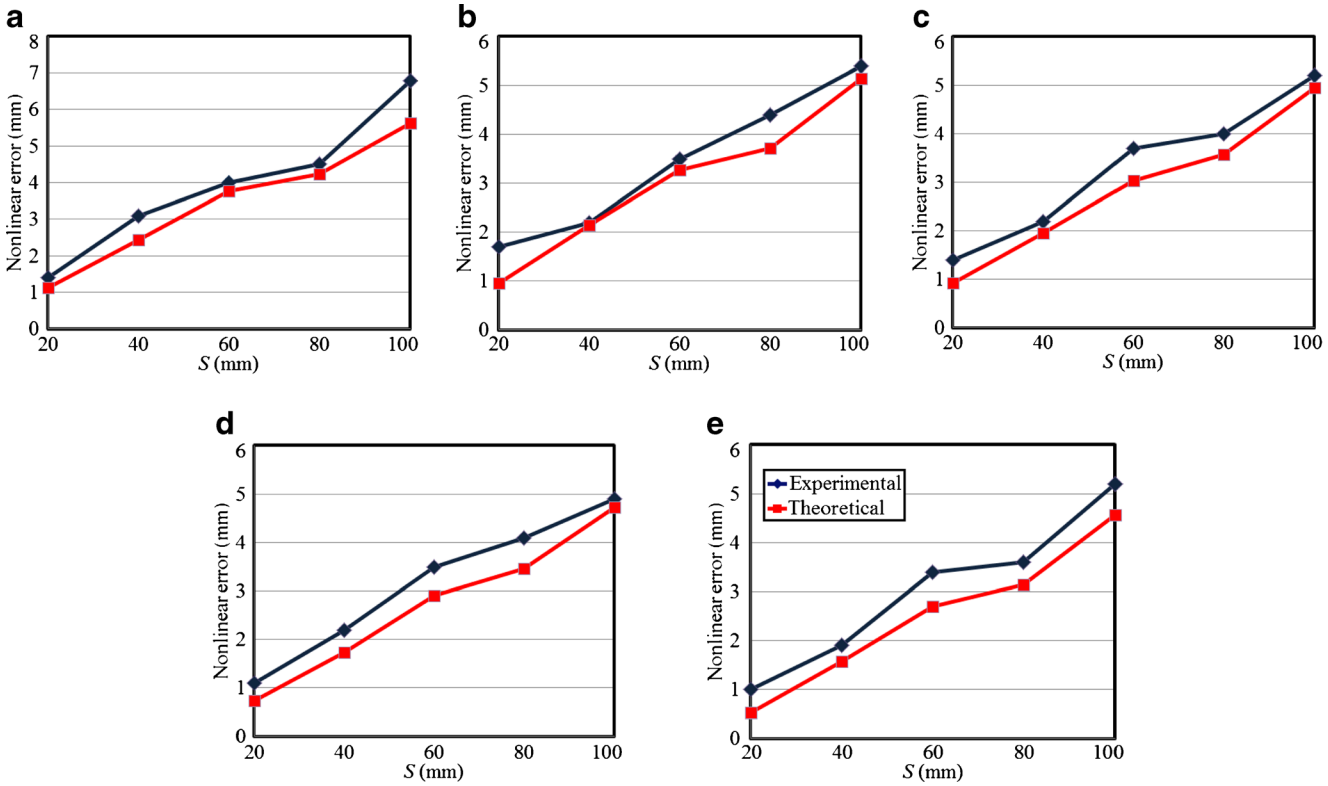

Fig. 8 Effects of changes in movement distance on error in platform motion by neglecting the rotational motion of the platform from areas 1 to 1: **a** X=100 mm, **b** X=200 mm, **c** X=300 mm, **d** X=400 mm, and **e** X=500 mm

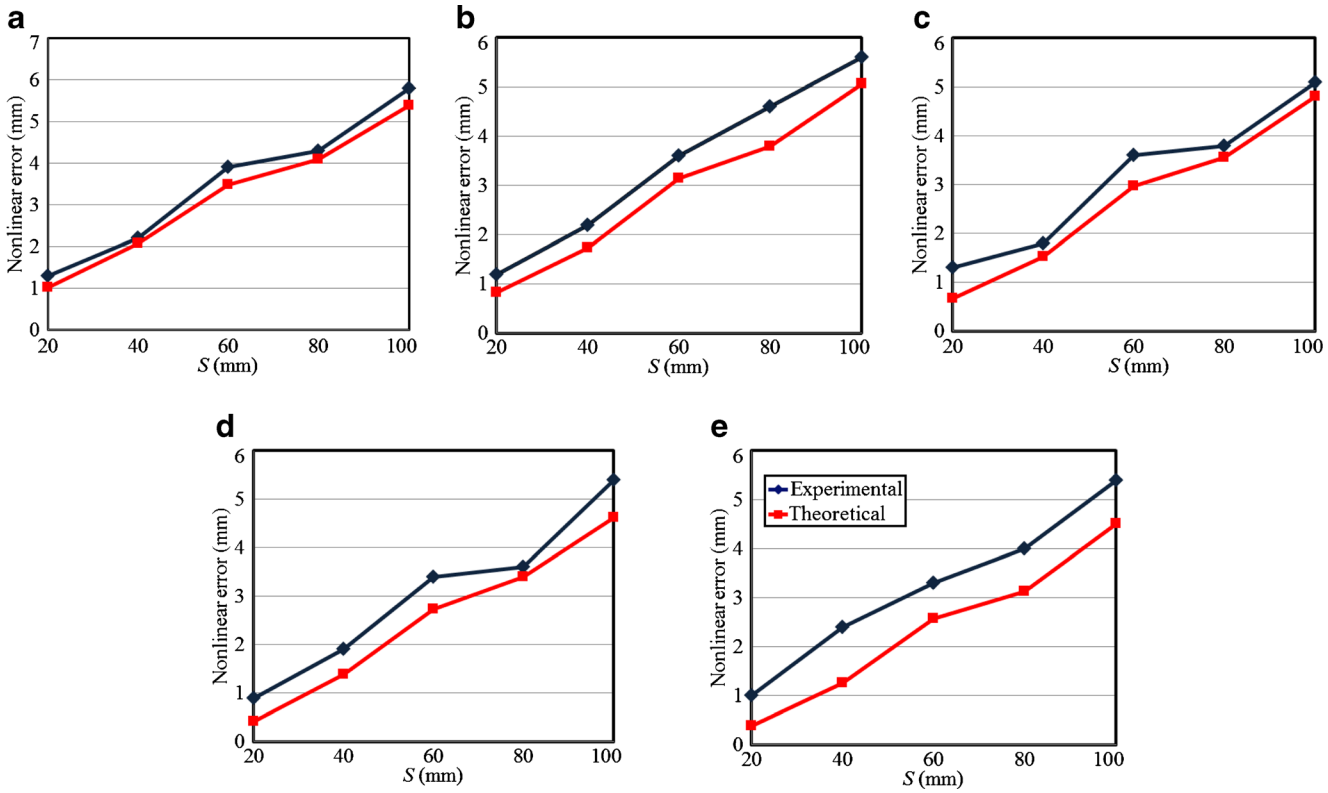

Fig. 9 Effects of changes in movement distance on error in platform motion by neglecting the rotational motion of the platform from areas 1 to 2: **a** X=100 mm; **b** X=200 mm; **c** X=300 mm; **d** X=400 mm; **e** X=500 mm

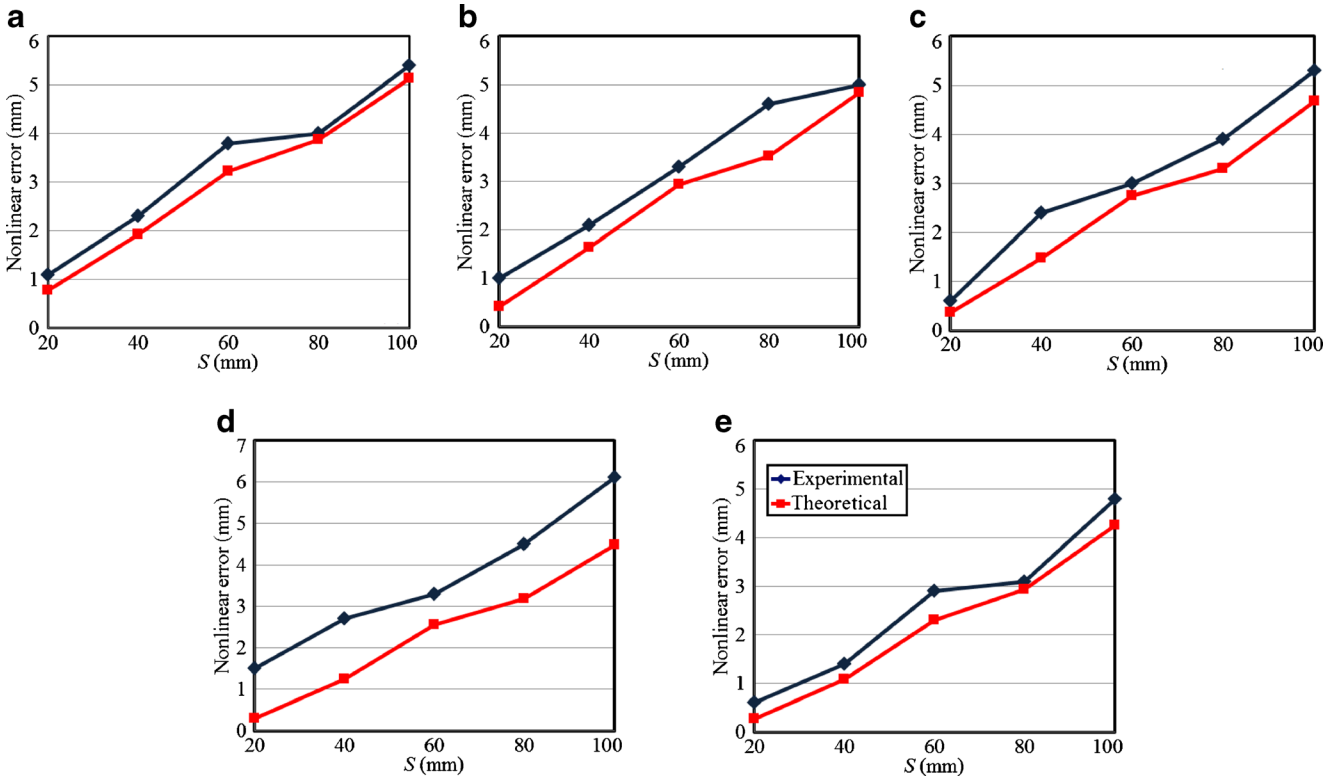

Fig. 10 Effects of changes in movement distance on error in platform motion by neglecting the rotational motion of the platform from areas 2 to 2: **a** X=100 mm, **b** X=200 mm, **c** X=300 mm, **d** X=400 mm, and **e** X=500 mm

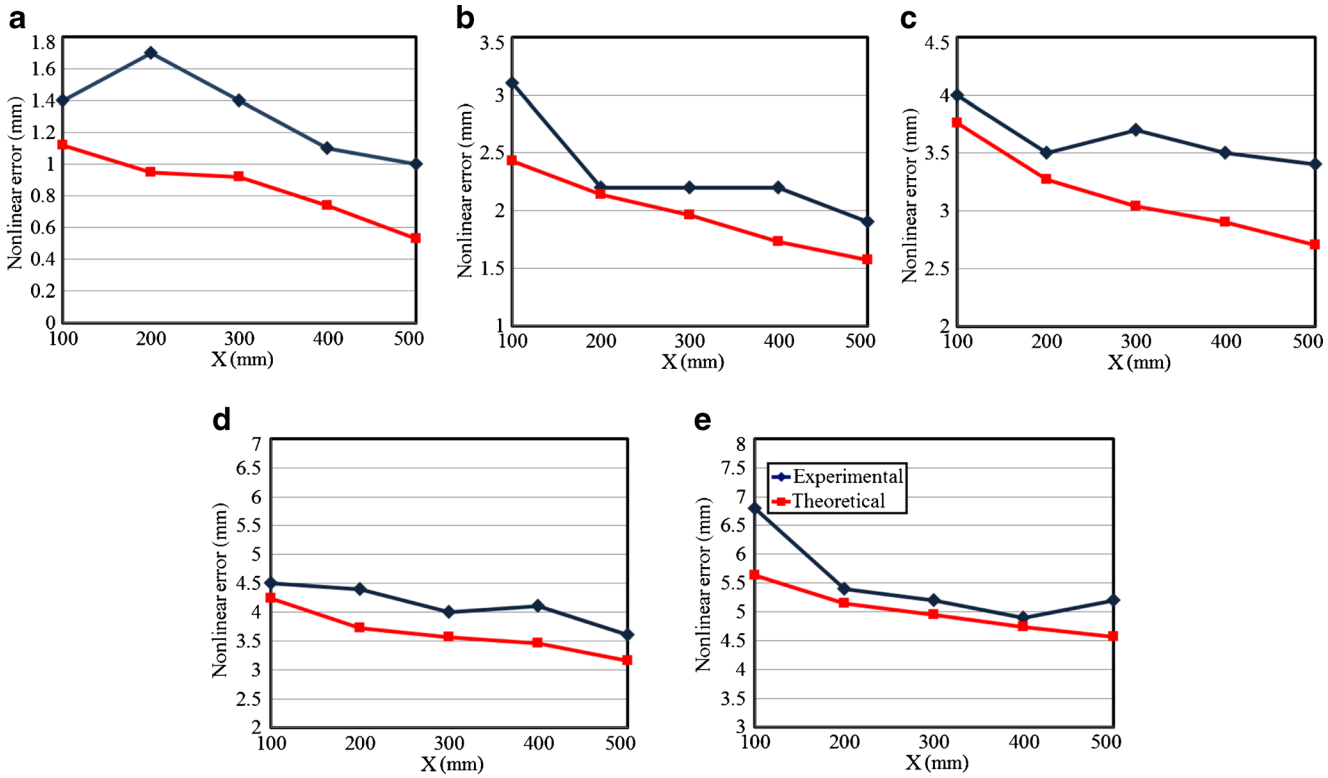

Fig. 11 Effects of changes in distance between the platform and base on motion error neglecting the rotational motion of the platform from areas 1 to 1: **a** S=20 mm, **b** S=40 mm, **c** S=60 mm, **d** S=80 mm, and **e** S=100 mm

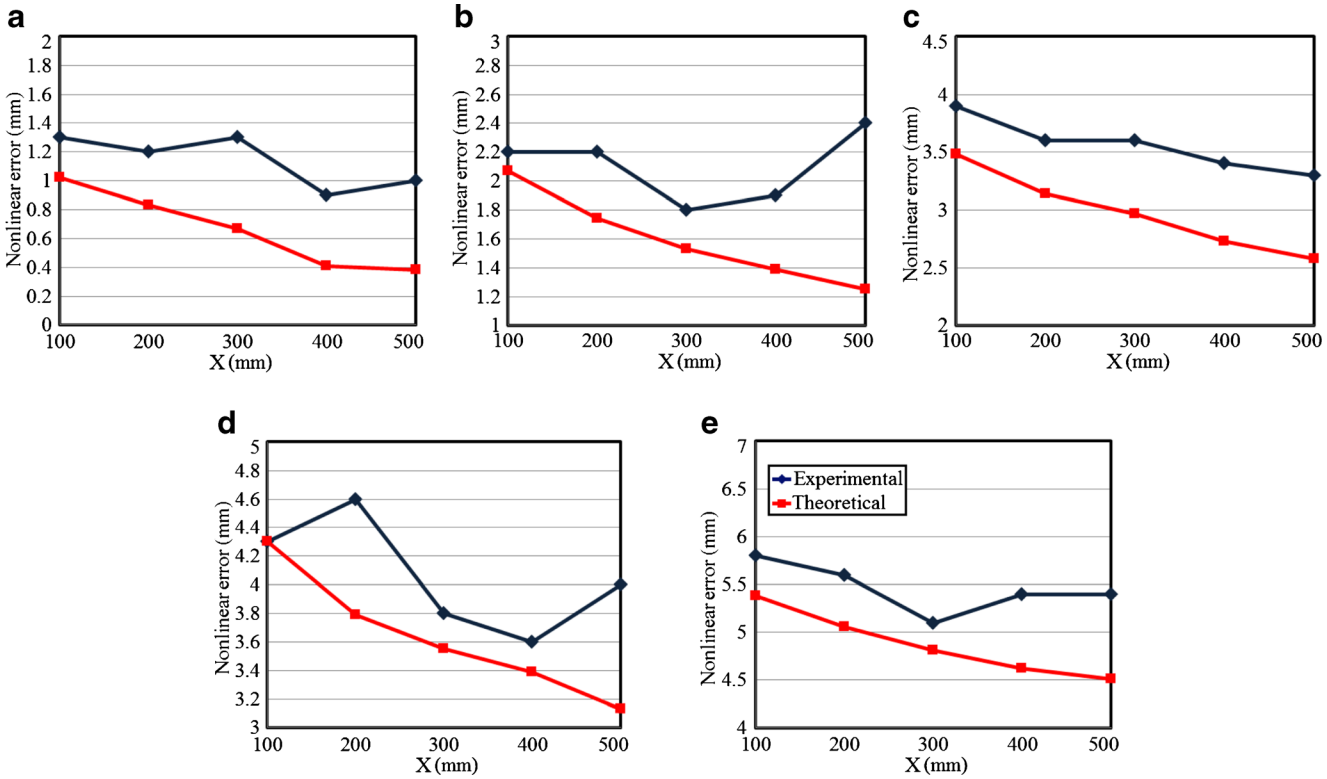

Fig. 12 Effects of changes in distance between the platform and base on motion error neglecting the rotational motion of the platform from areas 1 to 2: **a** S=20 mm, **b** S=40 mm, **c** S=60 mm, **d** S=80 mm, and **e** S=100 mm

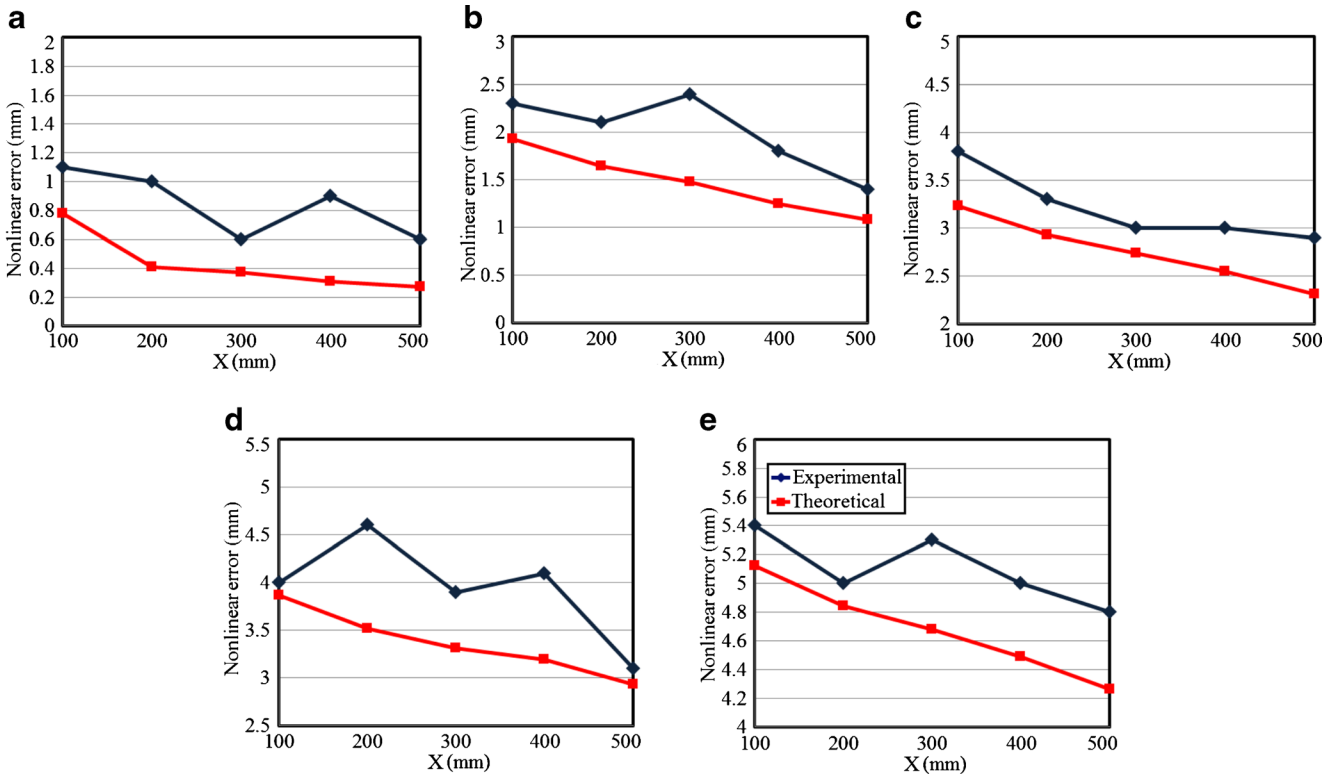

Fig. 13 Effects of changes in distance between the platform and base on motion error neglecting the rotational motion of the platform from areas 2 to 2: **a** S=20 mm, **b** S=40 mm, **c** S=60 mm, **d** S=80 mm, and **e** S=100 mm

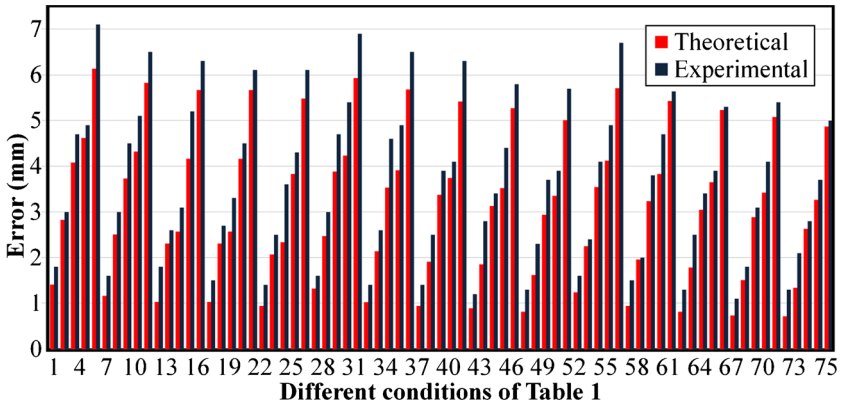

Fig. 14 Comparison of experimental and theoretical results taking into account the rotational motion of the platform

Figures 8 and 9 present the effects of the changes in movement distance, *S*, on error regardless of the platform's orientation. Regarding Figs. 8a–e, 9a–e, and 10a–e, it should be noted that the error increases by an increase in *S*. Moreover, it is obvious that the error in movement from areas 1 to 1 is larger to that of the platform movement from areas 1 to 2, and the error in movement from areas 1 to 2 is larger compared to that of the movement from areas 2 to 2.

Figures 11, 12, and 13 present the effects of changes in the distance of the platform from base, *X*, on error regardless of the platform's orientation. Regarding Figs. 11a–e, 12a–e, and 13a–e, it should be noted that the error decreases by an increase in *X*.

By considering the rotational motion of the platform, Fig. 14 illustrates the platform motion errors both theoretically and experimentally. In this bar chart, the maximum difference between the results obtained from theoretical and image processing is approximately 0.9 mm. The results of both methods are close to each other.

By taking the rotational motion of the platform into account, Figs. 15, 16, and 17 show the effects of the changes in movement distance, *S*, on error. Comparing Figs. 15, 16, and 17 with Figs. 8, 9, 10, and 11 makes it evident that error

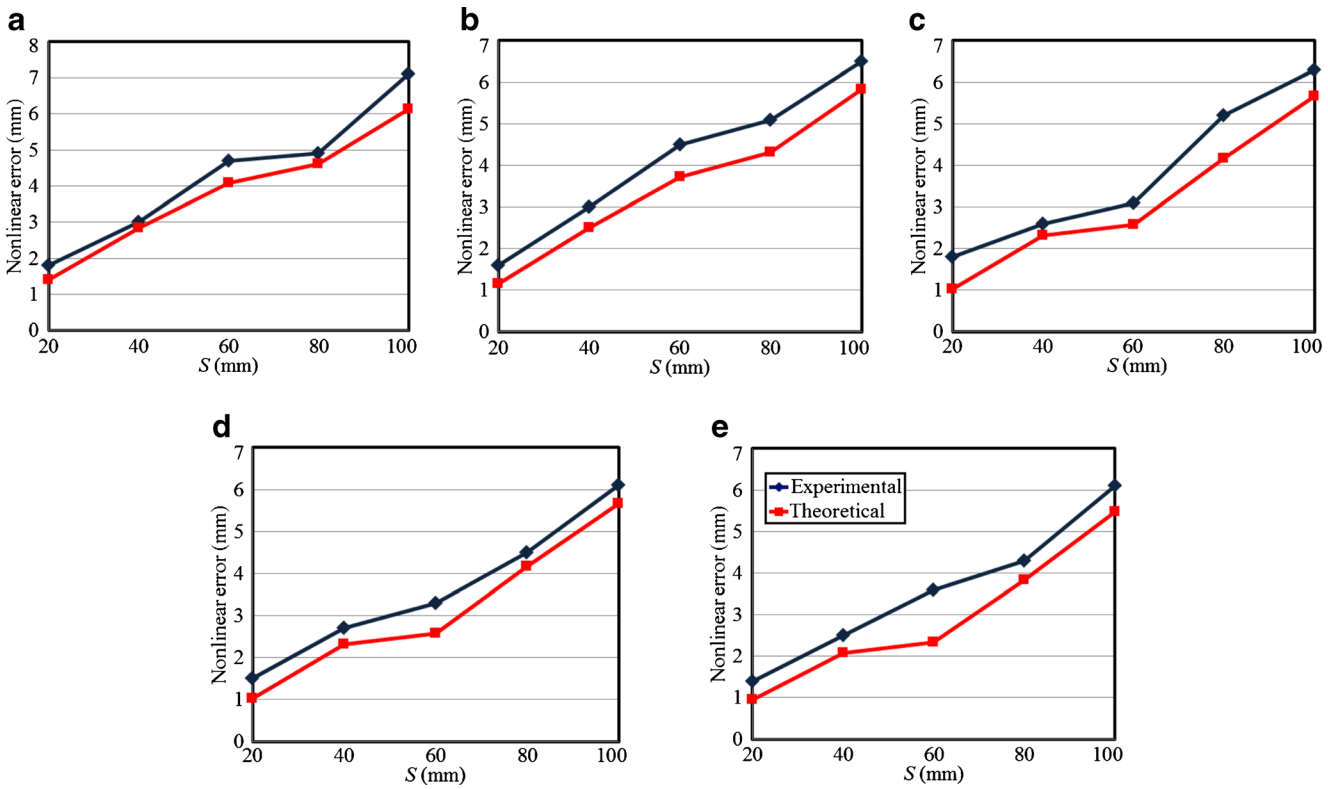

Fig. 15 Effects of changes in movement distance on error in platform motion considering the rotational motion of the platform from areas 1 to 1: **a** *X*=100 mm, **b** *X*=200 mm, **c** *X*=300 mm, **d** *X*=400 mm, and **e** *X*=500 mm

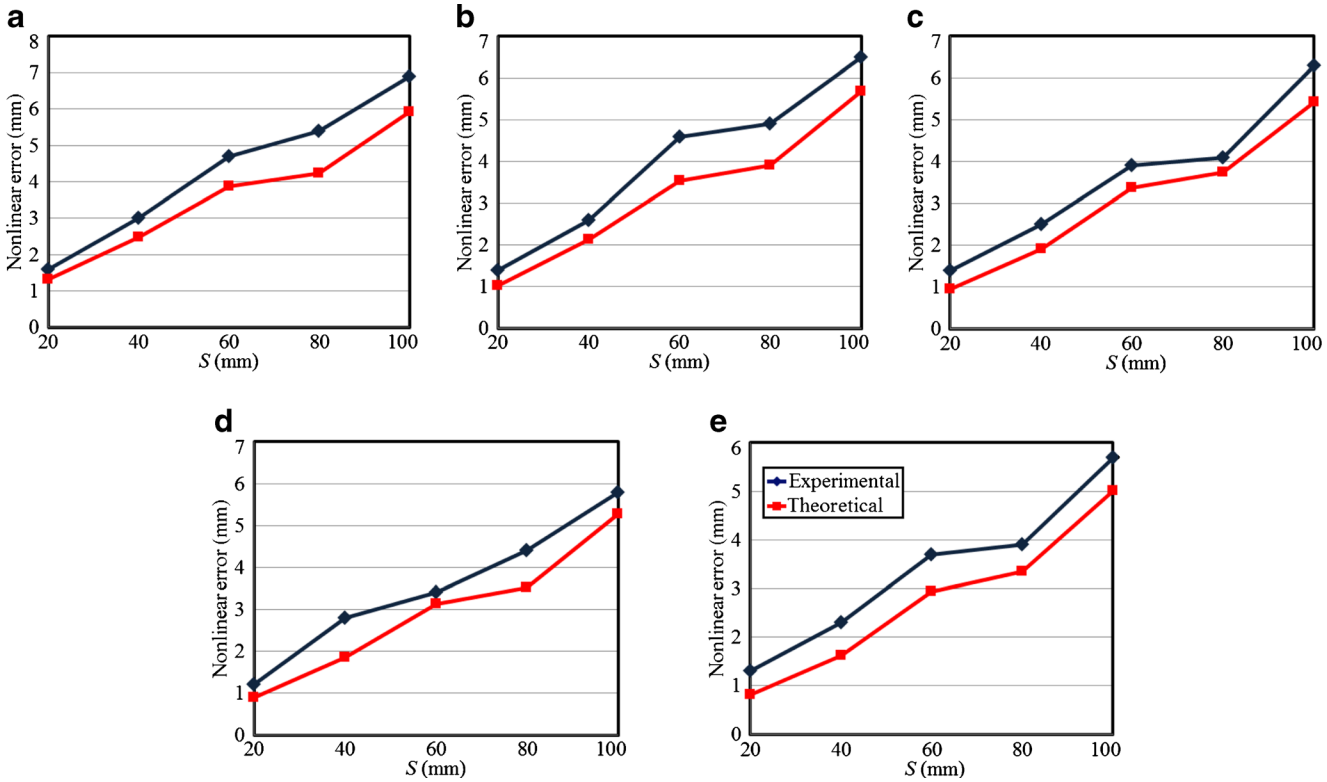

Fig. 16 Effects of changes in movement distance on error in platform motion considering the rotational motion of the platform from areas 1 to 2: **a** X=100 mm, **b** X=200 mm, **c** X=300 mm, **d** X=400 mm, and **e** X=500 mm

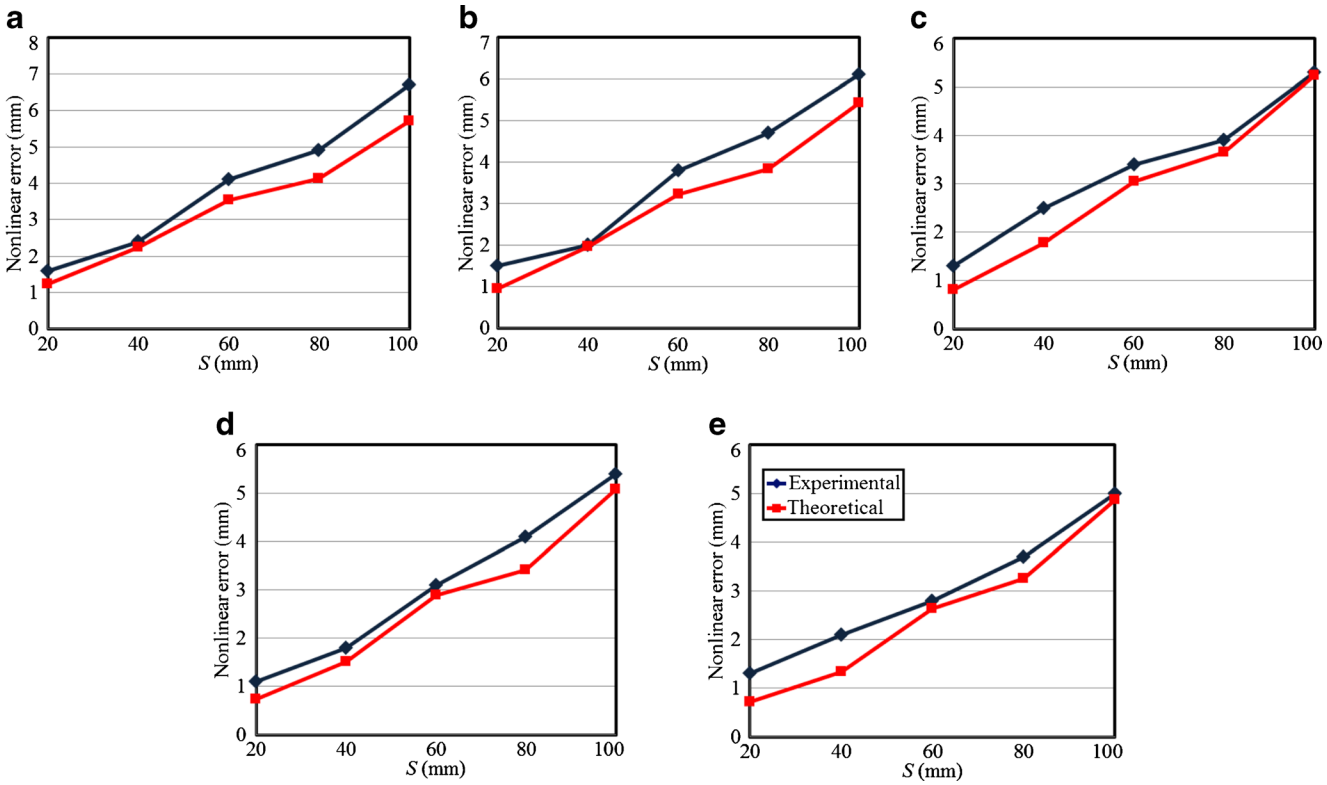

Fig. 17 Effects of changes in movement distance on error in platform motion considering the rotational motion of the platform from areas 2 to 2: **a** X=100 mm, **b** X=200 mm, **c** X=300 mm, **d** X=400 mm, and **e** X=500 mm

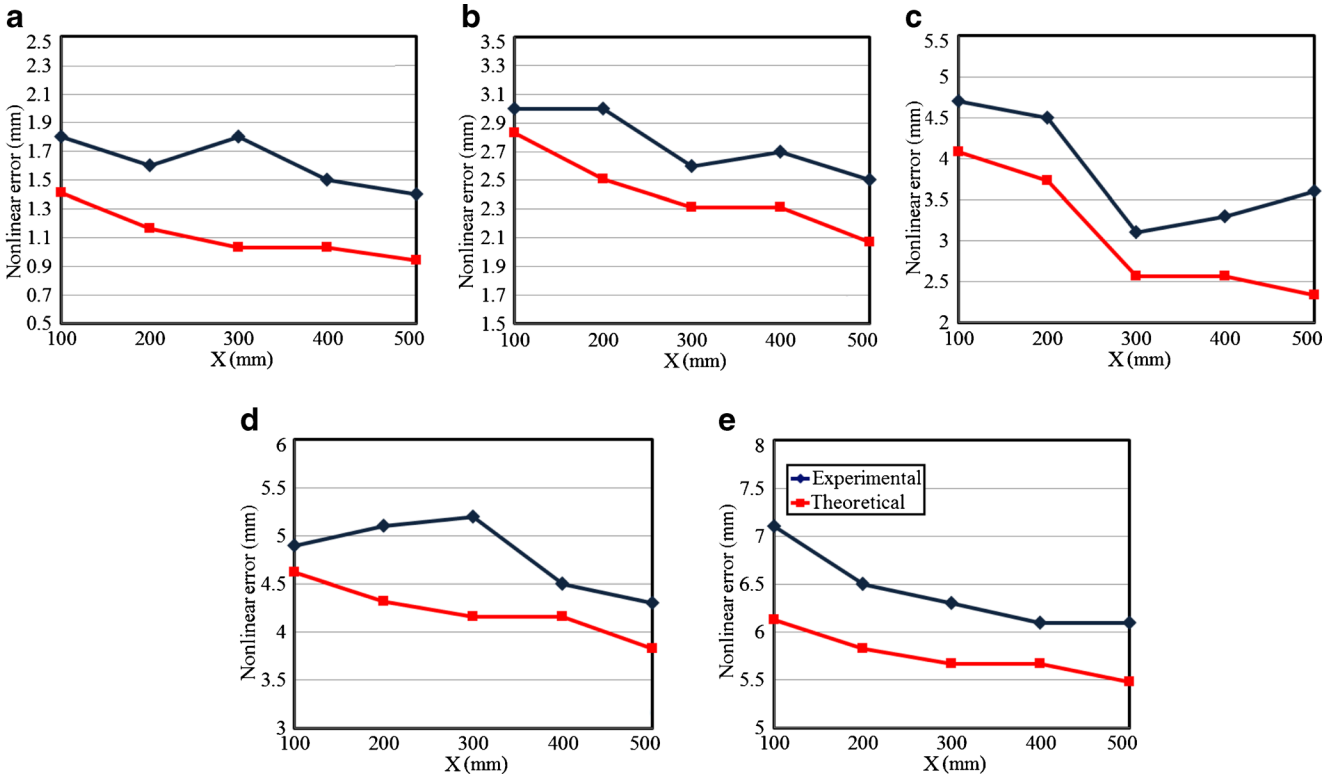

Fig. 18 Effects of changes in distance between platform and base on motion error considering the rotational motion of the platform from areas 1 to 1: **a** S=20 mm, **b** S=40 mm, **c** S=60 mm, **d** S=80 mm, and **e** S=100 mm

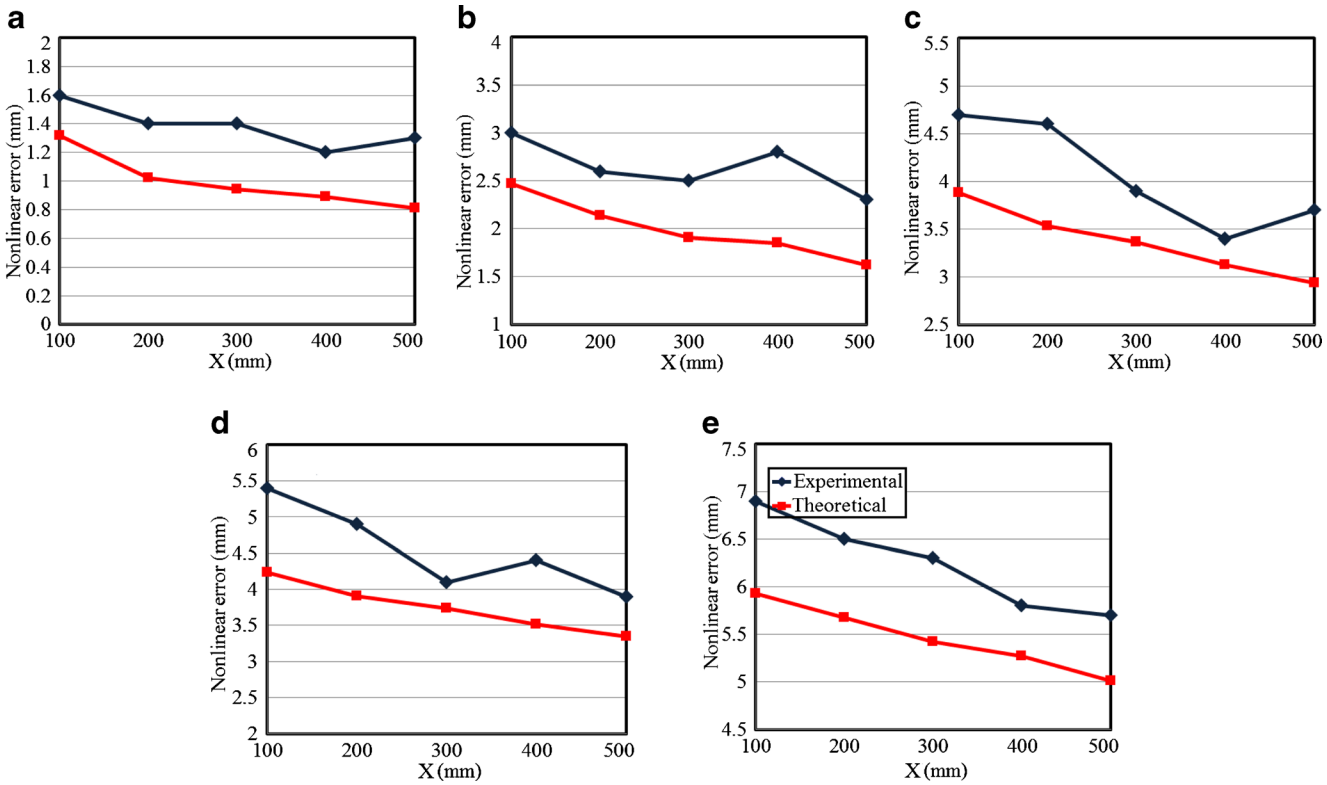

Fig. 19 Effects of changes in distance between the platform and base on motion error considering the rotational motion of the platform from areas 1 to 2: **a** S=20 mm, **b** S=40 mm, **c** S=60 mm, **d** S=80 mm, and **e** S=100 mm

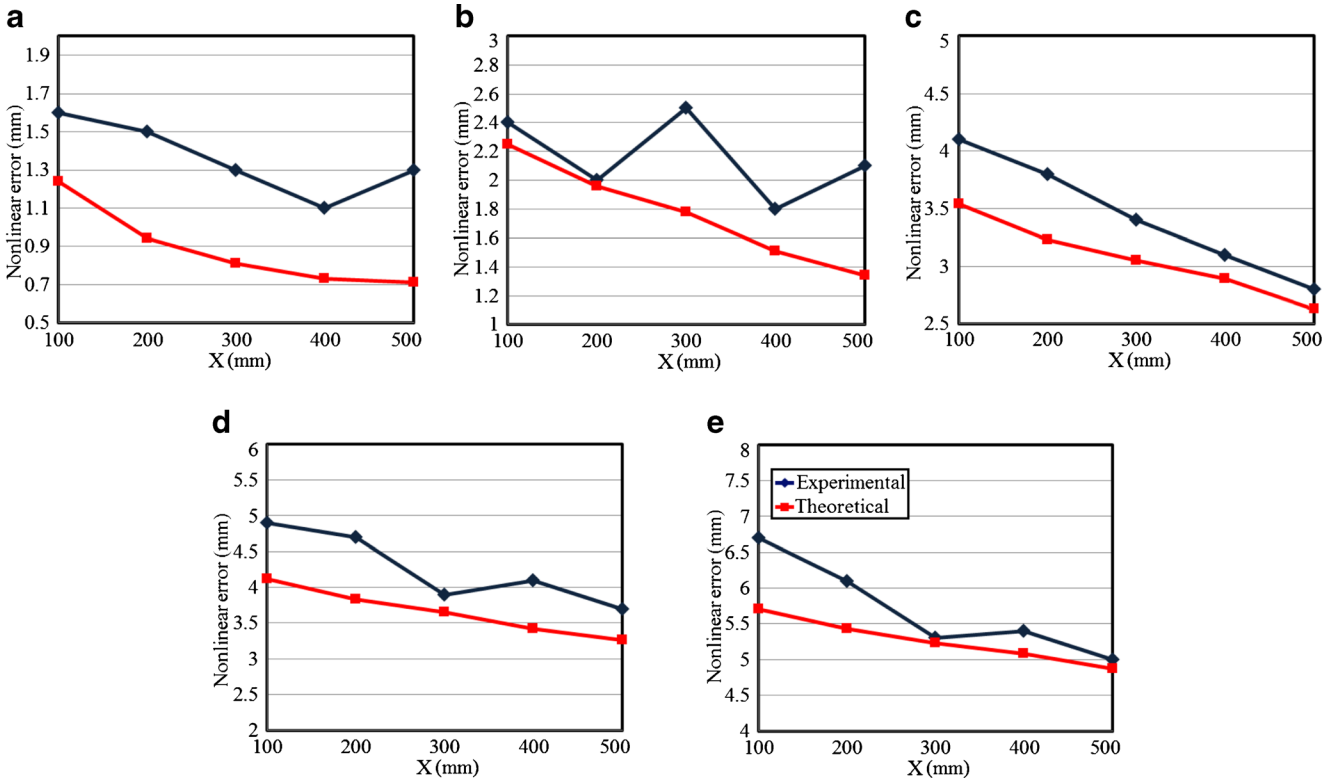

Fig. 20 Effects of changes in distance between the platform and base on motion error considering the rotational motion of the platform from areas 2 to 2: **a** S=20 mm, **b** S=40 mm, **c** S=60 mm, **d** S=80 mm, and **e** S=100 mm

increases by an increase in S where the platform's rotational motion is taken into consideration.

Figures 18, 19, and 20 present the effects of changes in the distance of the platform from the base, X, on error considering the platform's orientation. Comparing Figs. 18, 19, and 20 with Figs. 11, 12, and 13 makes it evident that error increases by an increase in X where the platform's rotational motion is considered.

8 Conclusions

In this study, a novel parallel mechanism with 6 degrees of freedom has been introduced and considered. Inverse and forward kinematic relations have been extracted. Using inverse and forward kinematics of position, movement error of the platform has been considered while moving from an initial position to a desired position and effective parameters have been determined. The results obtained by theoretical method have further been verified through experimental tests. It is found that the results of both analytical and experimental analyses are in agreement. Finally, it could be concluded that the error increases with increasing movement distance, and nonlinear error for the platform's motion in closer distances of platform from the base is more than that of larger distances. Furthermore, the error in movement from areas 1 to 1 is the largest, whereas in movement from areas 2 to 2, the error is the smallest. Changes in the orientation of the platform during motion lead to a more nonlinear error.

Appendix

The physical specifications of the test manipulator are as follows (all the quantities are given in SI units):

$$a_i = 0.225; \quad l_i = 0.285;$$
$$s_1 = 0.12; \quad s_2 = 0.02;$$
$$h_1 = 0.1; h_2 = 0.15; h_3 = 0.325;$$
$$h_4 = 0.375; h_5 = 0.55; h_6 = 0.6$$

References

1. Zhang D (2010) Parallel robotic machine tools. Springer, Oshawa
2. Harib K, Srinivasan K (2003) Kinematic and dynamic analysis of Stewart platform-based machine tool structures. Robotica 21:541–554
3. Pedrammehr S, Mahboubkhah M, Pakzad S (2011) An improved solution to the inverse dynamics of the general Stewart platform. In:

Proc. of the 2011 I.E. international conference on mechatronics, ICM 2011, 5971317:392–397
4. Pedrammehr S, Mahboubkhah M, Khani N (2012) Improved dynamics equations for the generally configured Stewart platform manipulator. J Mech Sci Technol 26:711–721
5. Zheng K-J, Gao J-S, Zhao Y-S (2005) Path control algorithms of a novel 5-DOF parallel machine tool. In: Proc. of the IEEE international conference on mechatronics and automation, Niagara Falls, 3: 1381–1385
6. Beale EML (1960) Confidence regions in non-linear estimation. J R Stat Soc Ser B 22:41–88
7. Guttman I, Meeter DA (1965) On Beale's measures of nonlinearity. Technometrics 7:623–637
8. Box MJ (1971) Bias in nonlinear estimation. J R Stat Soc Ser B 33: 171–201
9. Gillis R, Ratkowsky DA (1978) The behavior of estimators of the parameters of various yield-density relationships. Biometrics 34: 191–198
10. Bates DM, Watts DG (1980) Relative curvature measures of nonlinearity. J R Stat Soc Ser B 42:1–25
11. Karimi D, Nategh MJ (2011) A statistical approach to the forward kinematics nonlinearity analysis of Gough-Stewart mechanism. J Appl Math 2011:1–17
12. Dasgupata B, Mruthyunjaya TS (1998) Singularity-free path planning for the Stewart platform manipulator. Mech Mach Theory 33: 711–725
13. Shaw D, Chen YS (2000) Cutting path generation of the Stewart-platform based milling machine using an end-mill. Int J Prod Res 39: 1367–1383
14. Merlet JP (2001) A generic trajectory verifier for the motion planning of parallel robots. ASME J Mech Des 123:509–515
15. Pugazhenthi S, Nagarajan T, Singaperumal M (2001) Optimal trajectory planning for a hexapod machine tool during contour machining. Proc Inst Mech Eng C J Mech 216:1247–1257
16. Dash AK, Chen IM, Yeo SH, Yang G (2005) Workspace generation and planning singularity-free path for parallel manipulators. Mech Mach Theory 40:776–805
17. Afroun M, Chettibi T, Hanchi S (2006) Planning optimal motions for a DELTA parallel robot. In: Proc of the IEEE 14th Mediterranean conference on control and automation, pp 1–6
18. Afroun M, Chettibi T, Hanchi S, Dequidet A, Vermeiren L (2008) Optimal motions planning for a GOUGH parallel robot. In: IEEE 16th Mediterranean conference on control and automation, Congress Centre, Ajaccio, France
19. Harib KH, Sharif Ullah AAM, Hammami A (2007) A hexapod-based machine tool with hybrid structure: kinematic analysis and trajectory planning. Int J Mach Tools Manuf 47:1426–1432
20. Li Z (2000) Reconfiguration and tool path planning of hexapod machine tools. PhD thesis, New Jersey Institute of Technology, New Jersey
21. Jinsong W, Zhonghua W, Tian H, Whitehouse DJ (2002) Nonlinearity for a parallel kinematic machine tool and its application to interpolation accuracy analysis. Sci China Ser A 45:625–637
22. Isaksson M, Brogårdh T, Watson M, Nahavandi S, Crothers P (2012) The octahedral hexarot-A novel 6-DOF parallel manipulator. Mech Mach Theory 55:91–102
23. Isaksson M, Watson M (2013) Workspace analysis of a novel six-degrees-of-freedom parallel manipulator with coaxial actuated arms. ASME J Mech Des 135:1–9
24. Liu K, Fitzgerald JM, Lewis FL (1993) Kinematic analysis of a Stewart platform manipulator. IEEE Trans Ind Electron 40:282–293
25. Wang L-C, Oen K-T (2002) Numerical direct kinematic analysis of fully parallel linearly actuated platform type manipulators. J Robot Syst 19:391–400